Preequilibrium neutron emission in deep-inelastic collisions of ^{86}Kr on ^{166}Er at 11.9 MeV/nucleon

I. Tserruya, A. Breskin, R. Chechik, Z. Fraenkel, S. Wald, and N. Zwang
Weizmann Institute of Science, Rehovot 76100, Israel

R. Bock, M. Dakowski, A. Gobbi, and H. Sann
Gesellschaft für Schwerionenforschung, D-6100 Darmstadt, West Germany

R. Bass,* G. Kreyling, R. Renfordt, K. Stelzer, and U. Arlt
Institut für Kernphysik, University of Frankfurt, D-6000 Frankfurt, West Germany
(Received 29 March 1982)

Neutrons emitted in the deep inelastic collisions of ^{86}Kr on ^{166}Er at 11.9 MeV/nucleon, were measured in coincidence with both fragments. The velocity and angular distributions of the neutrons cannot be accounted for by assuming only isotropic evaporation from the fully accelerated fragments. The experimental analysis shows the presence of a preequilibrium component of neutrons emitted mainly on the side of the light fragments in quasielastic events, and on the side of the heavy fragments in strongly damped events. The qualitative features of the data are reproduced by a simple model which assumes that $\sim 10\%$ of the neutrons are knocked out at an early stage of the collision along the direction of the nuclear motion. Except for the preequilibrium component the neutron multiplicities are in good agreement with the predictions of evaporation model calculations.

NUCLEAR REACTIONS ^{166}Er(^{86}Kr,A_L)A_H, $E_{lab}=1.02$ GeV; $35 \leq A_L \leq 126$, $\theta_{lab}=6°-28°$; E_n, θ_n, ϕ_n in coincidence with fragments; deduced c.m. neutron energy spectra, neutron multiplicities; evidence for preequilibrium neutron emission.

I. INTRODUCTION

The emission of light particles, which accompanies the deep inelastic reactions, provides important information about the reaction mechanism. Of particular interest are the onset and the characteristics of preequilibrium particle emission. Recently a number of investigations have been published in which neutrons, protons, or alpha particles were measured in coincidence with deep inelastic fragments in both heavy[1-9] and light[10-23] mass systems. The main purpose of these measurements was to identify light particles emitted from the composite system prior to the separation of the two massive fragments. The experimental task is simpler in heavy systems, since the highly excited fragments predominantly decay by neutron emission and then only one type of light particles has to be measured. Detailed studies of the neutron emission have been performed for several heavy systems, ^{86}Kr+^{166}Er,[1,2] ^{56}Fe+^{165}Ho,[3] ^{63}Cu+^{197}Au,[4] and ^{132}Xe+^{197}Au,[5] at energies up to 8.5 MeV/nucleon. No evidence for preequilibrium effects was found in these studies. It was clearly shown that (i) the dissipated energy is shared between the fragments in proportion to their mass, i.e., the composite system reaches thermal equilibrium during the short interaction time, and (ii) the neutrons are statistically evaporated from the fully accelerated fragments. Several investigations have also been performed on the α-particle emission in similar heavy systems and at comparable incident energies, like ^{32}S+^{197}Au,[6] ^{86}Kr+^{197}Au,[7] ^{40}Ar+^{116}Sn, ^{154}Sm, ^{164}Dy, and ^{197}Au.[8] In contrast to the neutron data, the α-particle emission in these reactions could not be explained in terms of statistical evaporation from the fully accelerated fragments. This marked difference in the mechanism of neutron and α-particle emission is an interesting question.[9]

In lighter systems the experimental situation is more confused. The experimental data are generally characterized by a strong forward peak of relatively high-energy light particles. However, there is no consistent picture concerning the dominant mechanism of particle emission. Several studies of neutron and charged-particle emission in light col-

liding systems (generally with projectiles like B, C, N, or O) have been interpreted in terms of preequilibrium emission.[10–15] On the other hand, results from many other studies of similar or even identical systems were shown to be consistent with statistical evaporation from the fully accelerated fragments.[16–23]

Together with this large amount of data, many theoretical models have been developed for preequilibrium light particle emission. A variety of phenomenological approaches have been proposed whose common feature is the production of high-energy particles with velocities larger than the velocity of the projectile. In the hot-spot model,[24–27] high-energy tails are produced from a localized hot zone formed during the collision. In the Fermi-jet or promptly emitted particles (PEP) models[28–30] the fast particles are created by the coupling of the intrinsic nucleon Fermi motion to the relative motion of the nuclei. In the piston model[31,32] the fast particles are produced by the radial component of the friction force.

In the present work we report on a study of the neutron emission in deep inelastic collisions of ^{86}Kr on ^{166}Er at 11.9 MeV/nucleon. Neutron energy spectra were measured as a function of total kinetic energy (TKE), fragment mass, and fragment and neutron emission angles. The experimental setup which was used to detect neutrons in coincidence with the two complementary heavy reaction products is described in Sec. II. The method of data analysis is presented in Sec. III. The experimental results are presented and discussed in Sec. IV. They include differential cross sections of the mass, TKE, and angular distributions of the fragments, and velocity and angular distributions of the neutrons as function of TKE. Section IV also contains the c.m. energy spectra of the neutrons and the neutron multiplicities as a function of the mass and TKE of the fragments. They are compared with results from evaporation calculations. The data analysis shows that there is a relatively small component of preequilibrium neutrons which have a broad distribution of velocities centered around the velocity of the projectile. A simple picture of preequilibrium neutron emission which reproduces qualitatively the observed results is described in Sec. V. Based on this model the relative amount of preequilibrium neutrons observed in this work is estimated to be $\sim 10\%$ of the total number of emitted neutrons. A summary is given in Sec. VI. A preliminary report of this work was presented in Ref. 33.

II. EXPERIMENTAL ARRANGEMENT AND PROCEDURE

The essential feature of the experiment was the measurement of neutrons emitted in coincidence with the two complementary heavy reaction products. A pulsed beam of 11.9 MeV/nucleon ^{86}Kr produced by the Unilac accelerator at the Gesellschaft für Schwerionenforschung (GSI), Darmstadt, was used to bombard thin isotopically enriched targets of ^{166}Er. The reaction channel was identified by the kinematical coincidence technique. The light (L) and the heavy (H) fragments were detected in coincidence using position sensitive parallel-plate avalanche counters. The neutrons were detected in coincidence with the fragments in eight neutron detectors located at fixed angles. A schematic view of the experimental setup is shown in Fig. 1. We now consider in more detail each of the above elements of the experiment.

A. The pulsed beam

We made use of the bunched-beam facility of the Unilac which yielded beam pulses at 37 ns intervals with a width generally smaller than 250 ps. These pulses provided the reference timing signals for all time-of-flight (TOF) measurements. The position and width of the reference timing signal were continuously monitored by a small parallel-plate

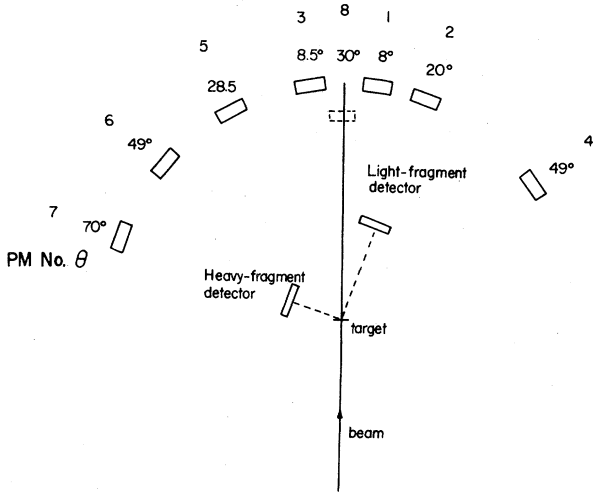

FIG. 1. Schematic view of the experimental setup. PM No. 8 was located in the vertical plane defined by the beam axis at an angle of 30° with respect to the beam. The other seven neutron counters were located in the equatorial plane.

avalanche counter, which measured beam particles scattered at forward angles by a thin carbon foil located 4 m downstream of the target. This information was periodically stored on magnetic tape and was used to correct for relative shifts of the reference timing signals, and to reject events accumulated during the time intervals (generally short) in which the quality of the pulsed beam deteriorated.

B. The targets and the scattering chamber

We used enriched ^{166}Er targets with an isotopic composition of 96.2% ^{166}Er, 2.8% ^{167}Er, and 1% of other stable Er isotopes. We used target thicknesses of 50 and 100 μg/cm^2 on a 25 μg/cm^2-thick carbon backing. The thinner targets were used in the measurements of quasielastic events in order to reduce the energy loss in the target of the low-energy targetlike fragments. It was necessary to apply to the targets a positive voltage of 20–25 kV in order to suppress the high background produced in the fragment detectors by electrons released from the target. The target was placed in the center of a spherical scattering chamber of 1 m diameter made of 3 mm-thick aluminum which was designed to minimize neutron scattering. Special precautions were taken in order to minimize the neutron scattering and the γ-ray background in the vicinity of the detection system: (i) Collimation of the beam by mechanical means was avoided; (ii) the concrete floor within a 3 m radius below the scattering chamber was replaced by a thin wooden floor; (iii) the beam stop was located at $\sim$8 m downstream of the target.

C. The heavy-ion detectors

The two heavy reaction products were detected in coincidence by position sensitive parallel-plate avalanche counters. The counters were very similar to those described in Ref. 34 with the difference being that we used delay-line readouts of the coordinates x, y instead of the charge-division technique. The H-fragment detector was operated with isobutane at a pressure of 6 Torr; it had a thin entrance window and a thin anode foil (total thickness of less than 200 μg/cm^2). These operating conditions ensured a $\sim$100% coincidence efficiency of the low-energy targetlike fragments produced in quasielastic events. The L-fragment detector was operated at a pressure of 12 Torr and with an entrance window and anode foil with a total thickness of 650 μg/cm^2. Each fragment detector provided five signals per event: the timing signal for the fragment TOF measurements, relative to the pulsed beam; two signals for the x coordinate (from each end of the delay line); and two signals for the y coordinate. The double information on the coordinates was used to reject the small fraction of events in which more than one fragment hit the detector. Both the L and the H fragment counters consisted of a pair of identical detectors each with a sensitive area of 10×8 cm^2 located above each other symmetrically with respect to the equatorial plane. This double counter arrangement was intended to yield information about the fragmentation of the L fragment.[35] In this paper the analysis is restricted to binary events only. This was ensured by accepting only twofold coincidence events with one fragment detected on one of the L counters and the other fragment on one of the H counters, and requiring that the fragment directions were coplanar with the beam axis (see Sec. III A).

In most measurements the L fragment counter was centered at $\theta=20°$, i.e., near the grazing angle ($\theta_g=17°$), and covered an angular range of 15° in plane and 23° out of plane. In order to achieve a complete kinematic overlap between the L and H fragments it was necessary to perform measurements with the H-fragment counter centered at $\theta=71°$, 50°, and 20°. These settings selected quasielastic, damped, and strongly damped events, respectively. At each angular setting the detector covered 26° in plane and 39° out of plane. Additional short measurements of quasielastic events were taken with the L-fragment counter centered at $\theta=14°$ and 17° and the H-fragment counter centered at $\theta=71°$.

The intrinsic resolutions of the detectors were the following: 200–250 ps time resolution, 2 mm and 5 mm in the x and y directions, respectively. The x and y resolutions were determined by the spacing of the wires in the central electrode and the width of stripes in the cathode, respectively.[34] The mass and energy resolutions in the present experiment were determined by the spread in velocity and angle imparted to the fragments by particle emission, rather than by the intrinsic resolution of the detectors. They were worse for lower TKE.

The position signals were calibrated by placing in front of the detectors a mask with holes of 1 mm diameter separated by 1 cm in both the horizontal and vertical dimensions. The internal time delay of the detectors was determined from a measurement of the elastic scattering of ^{86}Kr on ^{166}Er at 400 MeV.

D. The neutron counters

Neutrons were detected in coincidence with both fragments in eight neutron counters at fixed locations in space. The counters consisted of 5.1-cm-thick NE213 liquid scintillators of 11.3 cm diameter coupled to XP1040 photomultipliers. The counters were placed 90 cm from the target. Seven counters were located in the reaction plane and one counter was located at an angle of 30° above the reaction plane, in the vertical plane defined by the beam axis. The exact locations of the n counters are indicated in Fig. 1. The scintillators were covered by 3-mm-thick lead shields to reduce the γ-ray background. Three signals were derived for each particle detected in the neutron counters: (i) a TOF signal relative to the bunched beam, (ii) the pulse-height amplitude in the photomultiplier (PM), and (iii) a pulse shape signal which, together with the TOF signal, allowed a clear separation of neutrons and γ rays.

The neutron absorption produced by the fragment detectors in the different geometries was measured with use of a ^{252}Cf source. This absorption was always less than 15%. The absolute efficiency of the neutron counters was determined with use of the method of Drosg.[36] A 1.2 MeV neutron-energy threshold level was set off line on the pulse-height signal.

A typical TOF spectrum is shown in Fig. 2(a). The sharp peak at TOF=0 is the prompt γ peak. The combined time resolution of the scintillator and the beam pulse, as determined from the width of this peak, was 1 ns FWHM. The small peaks at 37 ns intervals are due to prompt γ rays emitted in previous or subsequent beam pulses and are indicative of the amount of random events. The true/random coincidences ratio was larger than 15/1. A clean separation between neutrons and γ rays was obtained in the two-dimensional display of TOF vs pulse shape signal as shown in Fig. 2(b). In such a display the neutrons and the γ rays appear along two separated bands. This display allows a further discrimination against delayed γ rays [such as those produced in $(n,n'\gamma)$ reactions] which appear as "neutrons" in the TOF spectrum.

E. Data acquisition

Events were recorded event by event on a PDP-11 computer with the aid of a CAMAC multiparameter data acquisition system.[37] Each fragment-fragment event in coincidence with at least one neutron detector was recorded on magnetic tape and was marked with a pattern word identifying the neutron counter. Only a fraction of the fragment-fragment events was recorded in order to minimize the dead time of the acquisition system. This fraction was varied from $\frac{1}{2}$ to $\frac{1}{20}$ depending mainly on the geometry of the fragment detectors.

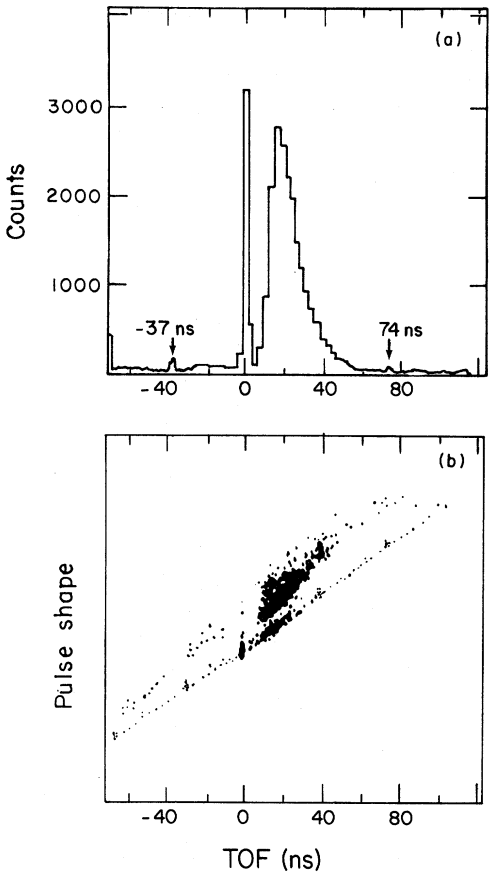

FIG. 2. (a) Typical neutron TOF spectrum. (b) Two-dimensional display of TOF vs pulse shape signal showing a clean separation between neutrons and γ rays.

III. DATA ANALYSIS

A. Mass and kinetic energy of the fragments

The analysis presented here was restricted to binary events, i.e., events in which only two massive fragments were emitted. The mass and kinetic energy of the fragments were then determined assuming two body reaction kinematics. This assumption is strongly supported by the results presented in Fig. 3 which shows the deviation from coplanarity be-

tween the L and H fragments ($\Delta\phi=\phi_L-\phi_H-180°$ where $\phi_{L,H}$ are the azimuthal angles of the fragments). Figure 3 also shows that the width of the distribution increases with decreasing TKE. This is due to the dispersion of the primary direction of the fragments produced by the emission of light particles.

We measured the scattering angles and velocities of both fragments although only three of those quantities are sufficient for the determination of the primary masses and kinetic energies. The H fragment had generally a very low energy (30 to 100 MeV) and thus large corrections had to be applied to its measured time-of-flight to account for the velocity losses in the target and the entrance window of the detector. To avoid these corrections the analysis was based on the measured scattering angles and the velocity of the fast fragment. It was shown[2] that this choice also minimizes the effect of the light particle emission on the mass and energy resolutions.

B. Neutron angular distribution and multiplicity

The angular distribution and velocity spectra of the neutrons were analyzed under the two following assumptions: (i) There are only two sources emitting neutrons, namely the L and the H fragment; and (ii) the neutrons are emitted isotropically in the c.m. system of the fully accelerated fragments. With these assumptions it is possible to reconstruct the neutron c.m. energy spectra of the two sources from the measured spectra of two neutron counters,

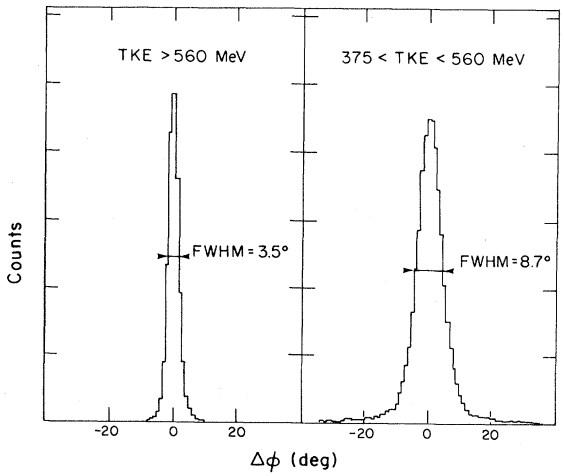

FIG. 3. Coplanarity for two different bins of TKE. $\Delta\phi=\phi_L-\phi_H-180°$, where $\phi_{L,H}$ are the azimuthal angles of the fragments.

which we will denote the "reference" counters. Generally for every neutron velocity in the c.m. system there are *two* velocities v_n for a fixed direction in the laboratory system. In principle, the c.m. spectrum can be determined from the high, the low, or both values of v_n. In this analysis we used the higher value of v_n since it provides the best accuracy. We used as reference counters PM No. 2 and PM No. 7, which were located near the L and H fragment directions, respectively. An iterative procedure was used to correct for neutrons detected in PM No. 2 (7) which were emitted by the H (L) fragment.[38] This iterative correction is important for the low-TKE events. The c.m. spectra were then projected back into the laboratory system to predict the neutron velocity spectra at the locations of the other neutron counters. The comparison of these projected spectra with the measured ones is used to verify our assumptions. A more detailed description of the analysis procedure is given in the Appendix.

The neutron multiplicities were calculated as a function of the mass and TKE of the fragments, from the total yield of neutrons emitted by the L and H fragments (as obtained from the reference counters), and from the total fragment yield.

The angular distribution and the velocity spectra of the neutron for the eight neutron counters were obtained as a function of the total kinetic energy of the fragments and summed over all L-fragment masses $A_L<126$. The threshold in the neutron c.m. energy depends on the relative angle between the directions of the fragment and the neutron. In order to minimize the threshold in the reference counter PM No. 2 with respect to the other neutron counters, all the neutron results presented in this work were obtained with the restriction $\theta_L\geq 14°$, where θ_L is the detection angle of the L fragment.

The fragment velocities and directions were corrected for the recoil momenta imparted to them by detected neutrons. However, the effect of the angular distribution[17,19,20] was not taken into account in the projected data. This effect is very important for alpha-particle emission from projectile-like fragments in ^{16}O induced reactions, as it was demonstrated in Refs. 17 and 20. However, it is negligible in the present system in which the average recoil angle imparted to the L fragment by neutrons detected in the reference counter PM No. 2 is 0.05° for quasielastic events and increases to 0.07° for strongly damped events. Moreover, the effect of the angular distribution is effectively taken into account by the large area of the L-fragment detector.

With a Monte Carlo simulation code (similar to

the one described in Sec. V, but without preequilibrium neutrons) we determined that this analysis procedure introduces systematic errors $\lesssim 5\%$.

IV. EXPERIMENTAL RESULTS AND DISCUSSION

A. Mass, TKE, and angular distributions of the fragments

The fragment angular distributions in the c.m. system are presented in Fig. 4 as function of the L-fragment mass (in bins of 8 u) and of TKE (in bins of 80 MeV). The absolute cross sections were obtained by normalizing the elastic scattering at the most forward angles to the Rutherford cross sections. The uncertainty in the absolute cross sections is estimated to be 20%. The angular distributions are strongly forward peaked for quasielastic events. With decreasing TKE or increasing mass transfer they become less steep and approach a $1/\sin\theta$ distribution for strongly damped events. The results are presented in Fig. 5 in the form of a Wilczynski plot. The hatched area indicates the kinematic cuts of the detectors.

The mass and TKE distributions are shown in Fig. 6. Both distributions are characterized by (i) a strong quasielastic peak (a peak at the c.m. energy of 674 MeV in the TKE distribution, and a sharp peak at the projectile mass, in the mass distribution), since a large fraction of the detector area covered angles below the grazing angles; and (ii) a broad distribution of strongly damped events, centered at ~ 200 MeV in the TKE distribution, and nearly flat in the mass distribution, with mass transfers up to 40 u.

B. Neutron angular distributions

The measured (i.e., not corrected for efficiency and for the neutron absorption produced by the fragment detectors) neutron angular distributions in the laboratory system are shown in Fig. 7 for four bins of TKE. Positive (negative) angles refer to the side of the beam where the L (H)-fragment detector was located. The lines in Fig. 7 represent the calculated yield based on the reference counters.

The angular distributions are forward peaked on the side of the L-fragment detector. This peak is produced by the neutrons emitted by the L fragment which are strongly focused in the laboratory system by the high velocity of the L fragment. For

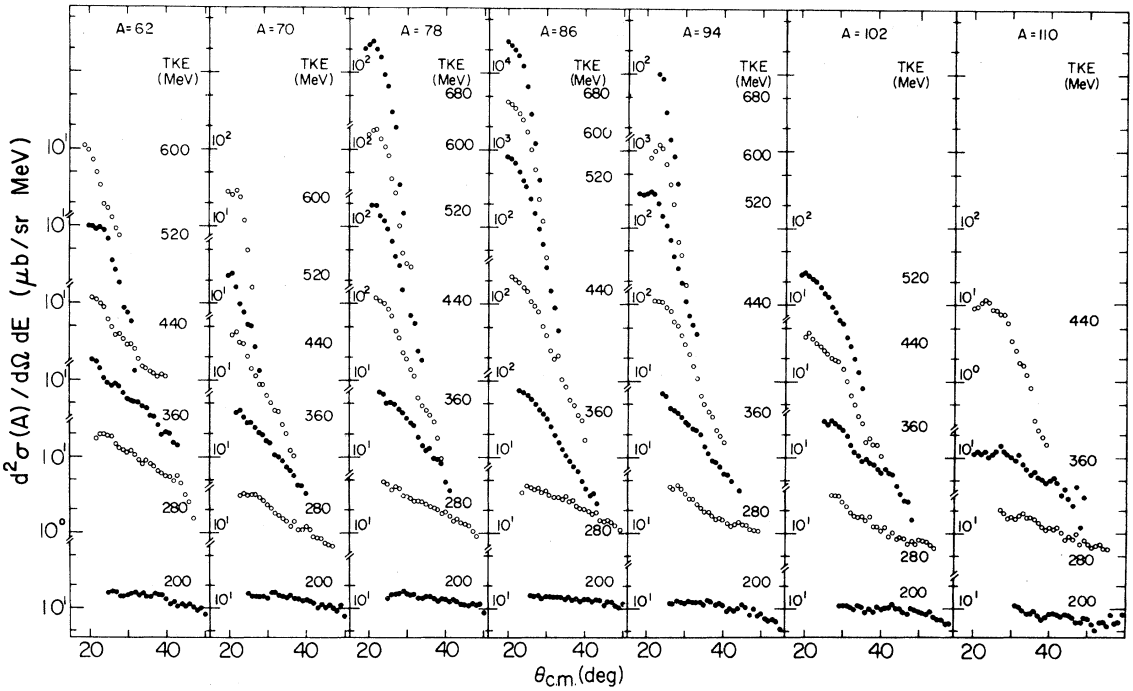

FIG. 4. Differential cross sections as a function of the c.m. scattering angle of the L fragment for ^{86}Kr on ^{166}Er at 11.9 MeV/nucleon. The cross sections are centered around the values indicated in the figure for the L-fragment mass (A) and total kinetic energy (TKE), and averaged over intervals of 8 u in mass and 80 MeV in TKE.

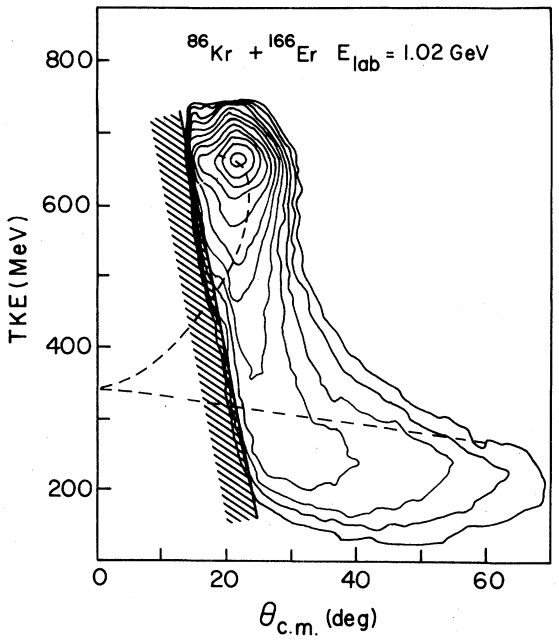

FIG. 5. Wilczynski plot of the reaction ^{86}Kr + ^{166}Er at 1.02 GeV. The hatched area indicates the kinematic cut of the detectors. The dashed line is a calculation based on a classical friction model (see Sec. V).

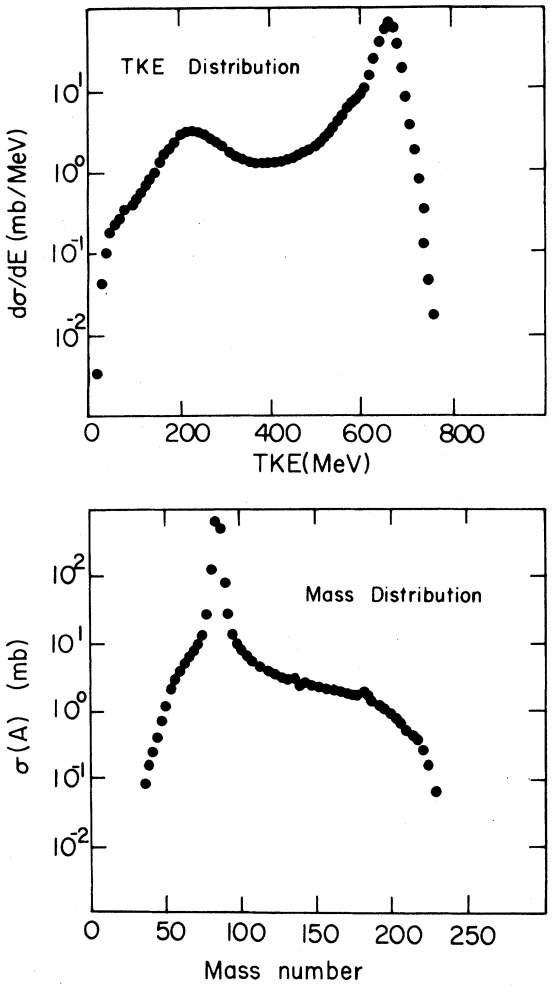

FIG. 6. Total kinetic energy distribution (upper part) and mass distribution (lower part) measured in the L detector. The cross sections are integrated over the angular range of the detectors and the different geometries of the experiment.

quasielastic events the H fragment has a very small velocity and thus the neutrons it emits have a nearly isotropic distribution in the laboratory. With decreasing TKE the velocity of the H fragment increases and the neutron emission from the H fragment is more focused in the direction of that fragment.

The large focusing effect of the L-fragment motion facilitates the separation of the contribution of the neutrons emitted by the two sources in the reference counters. It is seen in Fig. 7 that neutrons emitted by the L fragment do not reach the reference counter PM No. 7, located at $-70°$. Thus the yield measured in this counter gives the neutron emission from the H fragment only. A fraction of the neutrons detected in the reference counter PM No. 2, located at $+20°$, originates from the H fragment, and this fraction increases with decreasing TKE. The iteration procedure mentioned in Sec. III B allows us to determine the contribution of neutrons emitted by the L fragment (also see the Appendix).

The lines in Fig. 7 represent the calculated neutron yields based on the reference counters. The neutron emission from the L fragment (dashed lines in Fig. 7) is peaked at an angle close to or smaller than 20°. This is due to two main factors: (i) the focusing effect which produces a maximum at the average detection angle of the L fragment and (ii) the neutron absorption produced by the L-fragment detector. (The absorption factor was larger for PM No. 2 and PM No. 1 when the L-fragment detector was located at 20° and 14°, respectively. These two geometrical configurations contributed essentially to the data with TKE $>$ 560 MeV and TKE $<$ 560 MeV, respectively.)

The total calculated yield (solid lines in Fig. 7) reproduces the general trend of the data. However, two significant discrepancies are clearly seen. For quasielastic events (TKE $>$ 560 MeV) the calculations predict a smaller yield than observed experimentally at the forward angles. This discrepancy is also present at the reference counter located at

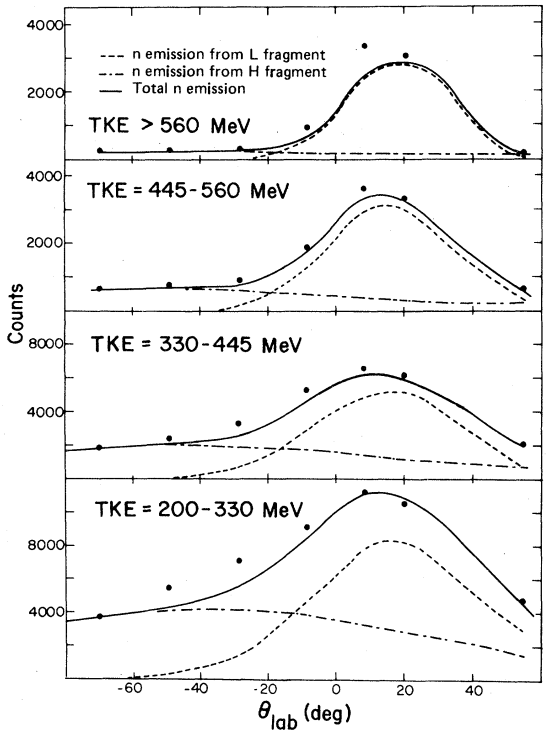

FIG. 7. Neutron angular distributions in the laboratory system for four bins of TKE, and for L-fragment mass $A_L < 126$. The dots denote the experimental yield. The dashed and dotted-dashed lines show the calculated yield of neutrons emitted by the L and the H fragment, respectively. The solid line represents the sum of these two contributions.

$+20°$. Since the calculations are based on the "high" velocity neutrons measured in this counter (see Sec. III B and the Appendix), this indicates that the measured spectrum is not consistent with symmetric emission of n around 90° in the rest frame of the L fragment. With decreasing TKE this discrepancy disappears and another effect builds up; the calculations predict a smaller yield than observed experimentally on the other side of the beam, close to the recoil direction of the H fragment. These discrepancies will be discussed in more detail in the next section.

C. Neutron velocity spectra

In this section we compare the measured neutron velocity spectra with the calculated ones based on the reference counters. Figures 8—10 show this comparison for only two neutron counters, PM No. 1 and PM No. 5, where the discrepancies are most prominent. A comparison for all the eight neutron

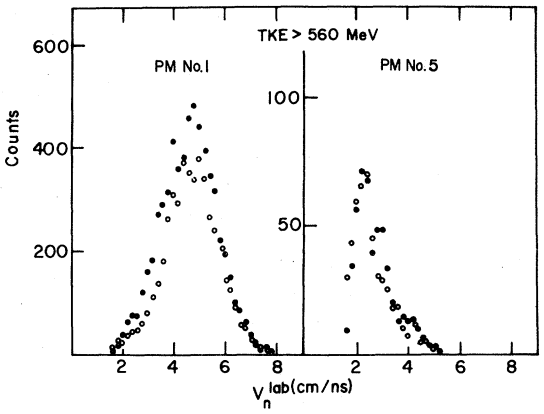

FIG. 8. Measured neutron velocity spectra (closed circles) for L-fragment mass $A_L < 126$ and for TKE > 560 MeV. The open points were calculated from the measured spectra in the reference counters, PM Nos. 2 and 7, assuming isotropic emission in the c.m. system of the fragments.

counters is given in Fig. 11 for the lowest TKE bin (200—330 MeV). The closed and open circles represent the directly measured and projected yields, respectively.

For TKE > 560 MeV most of the neutrons measured at forward angles are emitted by the L fragment. The two peaks observed in PM No. 1 in Fig. 8 correspond to forward and backward emission of neutrons in the rest frame of the L fragment which has a velocity nearly equal to the magnitude of the beam velocity $v_0 = 4.6$ cm/ns. With decreasing TKE the double structure disappears and the velocity spectra become broader as seen in Figs. 9—11 because of the large spread in velocity and angle of the L fragment. PM No. 5 is predominantly sensitive to neutrons emitted by the H fragment (see Fig. 7) which has a relatively low velocity ($v_H \leq 2$

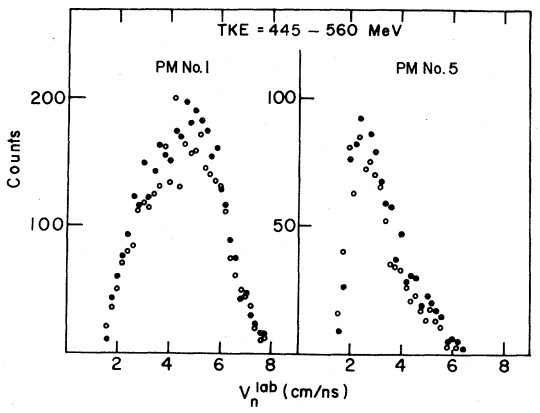

FIG. 9. Same as Fig. 8 for TKE = 445—560 MeV.

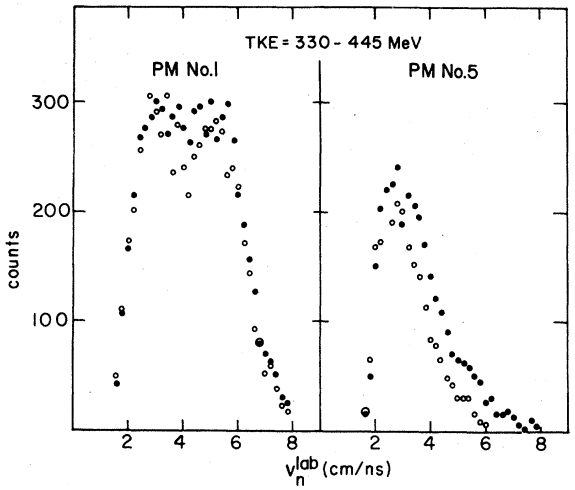

FIG. 10. Same as Fig. 8 for TKE=330−445 MeV.

cm/ns). The neutron velocity distribution in the laboratory system has a peak at low velocity which moves to higher values as the velocity of the H fragment increases with decreasing TKE (see Figs. 8−11).

The discrepancy seen in the neutron yield at forward angles for TKE > 560 MeV (Fig. 7) appears in PM No. 1 essentially at low neutron velocities, i.e., for $v_n \leq v_0$. The high velocity part of the spectrum is nicely reproduced by the calculations. For quasielastic events we therefore identify a small component of preequilibrium neutrons emitted close to the L-fragment direction and extending towards and beyond the beam direction (between $-8°$ and $+20°$). These neutrons may have small velocities $v_n \leq v_0$ as suggested by Fig. 8. It should, however, be noticed that the results are also consistent with preequilibrium neutrons having a broad velocity distribution centered around v_0. In such a case, the preequilibrium neutrons with $v_n > v_0$ cannot be seen in Fig. 8 because of the limitations of our analysis: As discussed in Sec. III B and in the Appendix, the predicted spectra are calculated from the high velocity neutrons measured in the reference counters, and therefore the preequilibrium neutrons with $v_n > v_0$ appear in PM Nos. 1 and 2 as "evaporated" neutrons.

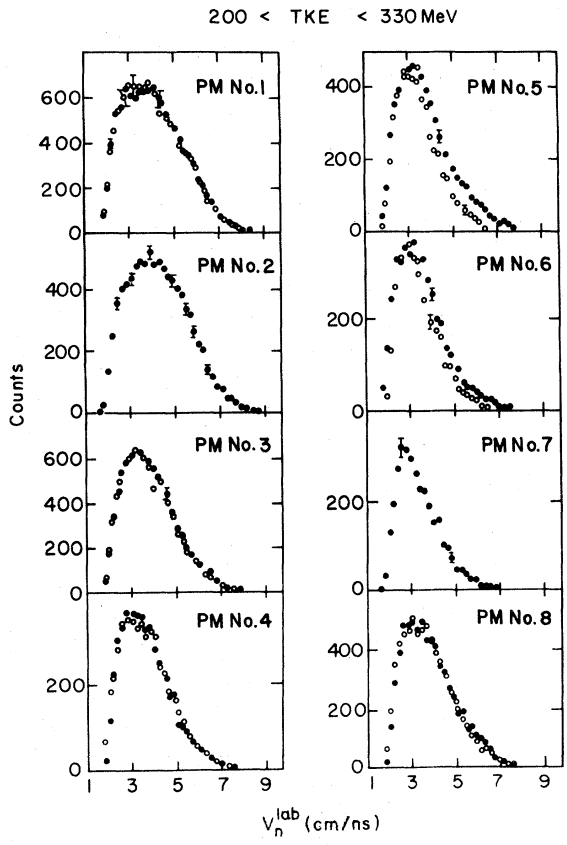

FIG. 11. Same as Fig. 8 for TKE=200−330 MeV.

The effect seen for quasielastic events at forward angles disappears with decreasing TKE and both the total yield (Fig. 7) and the velocity spectra (Figs. 9−11) of the forward counters are in good agreement with the calculations. For strongly damped events the calculations predict a smaller neutron yield in the counters PM Nos. 5 and 6 which are located near the recoil direction of the H fragment. Figures 10 and 11 clearly show that only the high velocity tail ($v_n > 3$ cm/ns) in these counters is not reproduced by the calculations. The effect is most pronounced for the lowest TKE bin (Fig. 11). As for quasielastic events, these results indicate that there is a component of preequilibrium neutrons with a broad velocity distribution centered at a value close to the beam velocity v_0.

For all cases in which the calculated total neutron yield agrees with the measured one (Fig. 7), the calculated velocity spectra are also in good agreement with the measured ones. An example is given in Fig. 11 which also includes the out-of-plane neutron counter.

D. c.m. neutron energy spectra

Figure 12 shows the c.m. energy spectra of neutrons emitted by the L and the H fragments as a function of TKE. These spectra were obtained from the reference counters PM Nos. 2 and 7 as explained in Sec. III B and in the Appendix. The spectra fall off nearly exponentially, characteristic of statistical decay. The equal slopes and thus equal temperatures of the two sources indicate that

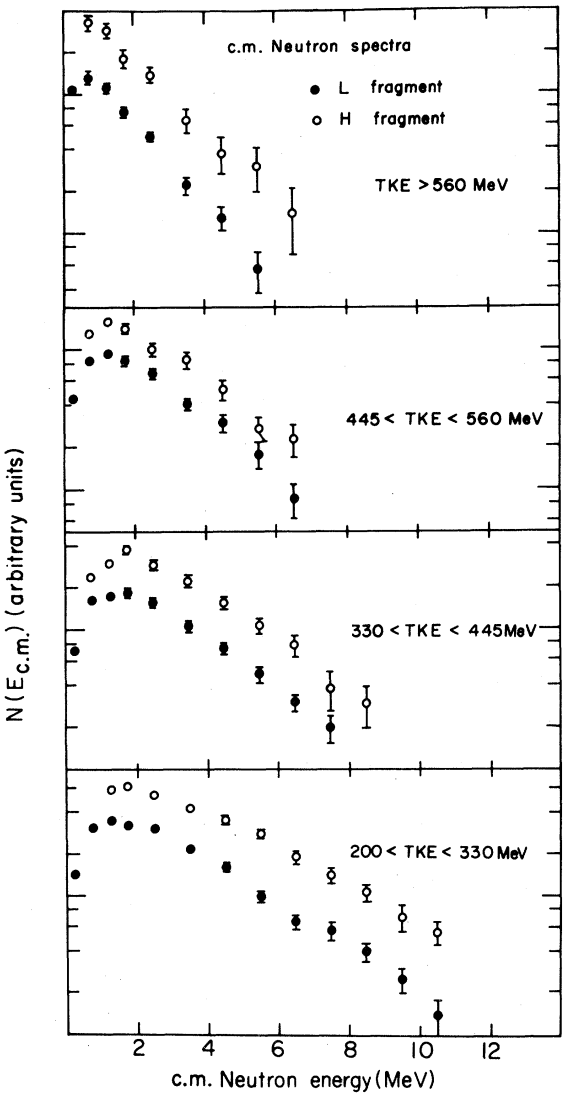

FIG. 12. The c.m. neutron energy spectra for four bins of TKE as obtained from the reference counters. The full circles represent neutrons emitted by the L fragment and the open circles represent neutrons emitted by the H fragment.

the excitation energy is shared between the fragments in proportion to their mass, i.e., the composite system is thermalized prior to the separation of the fragments. The same conclusion will also be obtained in the next section from the neutron multiplicity results. The slope decreases with TKE, reflecting the higher temperatures of the fragments as more kinetic energy is converted into excitation energy of the fragments.

It is important to understand why the preequilibrium neutrons discussed in the two previous sections do not manifest themselves in the c.m. spectra. First we notice that they represent only a small fraction of all neutrons emitted (of the order of 10% as will be shown in Sec. V), i.e., most of the data is in agreement with statistical emission of neutrons by the fully accelerated fragments. Second, our analysis shows that there is no evidence for the presence of preequilibrium neutrons in the reference counter PM No. 7. Only the reference counter PM No. 2 could detect the preequilibrium neutrons emitted in quasielastic events. Since these neutrons have velocities $v_n \leq v_0$ and the analysis is based on the "high" velocity component, they could affect the c.m. spectrum only at low c.m. energies. Therefore, the slope of the c.m. energy spectrum remains unaffected by the presence of the preequilibrium neutrons in the reference counter PM No. 2.

E. Neutron multiplicities and evaporation calculations

In the previous section we showed that the c.m. spectra derived from the high velocity component of the neutrons measured in the reference counters have the characteristic features of statistical evaporation. Here we consider this point more quantitatively by comparing the measured neutron multiplicities with results of evaporation calculations. The neutron multiplicities were obtained from the c.m. neutron yield deduced from the reference counters. The results are presented in Figs. 13 and 14 as function of the total excitation energy of the fragments and for various mass bins. The neutron multiplicity increases almost linearly with excitation energy up to 130–150 MeV. At higher excitation energies the neutron multiplicity increases much slower. The experimental errors in the neutron multiplicity are of the order of 10%; in the next section we show that the preequilibrium neutrons are of the same order. Thus the measured multiplicities are not affected by the small component of preequilibrium neutrons. The evaporation calculations were performed for the center value of the mass bin with the following assumptions: (i) For a given mass division the atomic number of the fragment was obtained assuming that its charge/mass ratio equals the charge/mass ratio of the composite system[39]; (ii) we assumed that the TKE loss, corrected for the ground-state Q value of the reaction, is fully converted into the excitation energy of the fragments; (iii) the total excitation energy is shared between the fragments in proportion to their mass.

We first consider the sensitivity of the calculations to the angular momentum of the fragments. We used the Monte Carlo code JULIAN[40] which

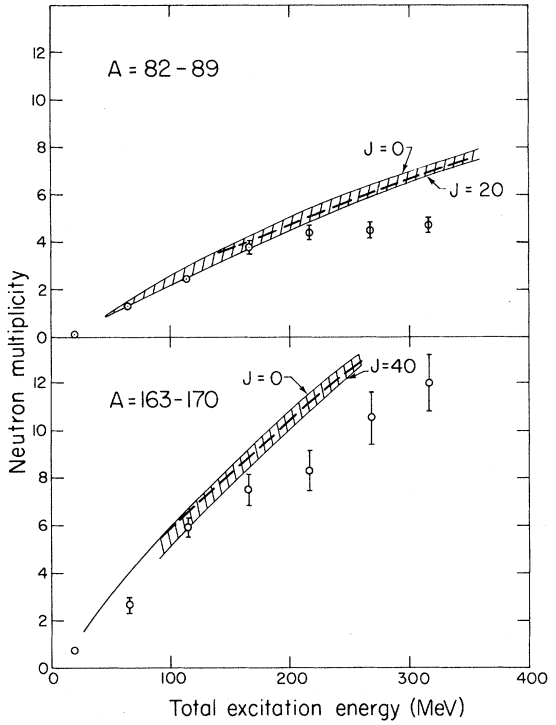

FIG. 13. Measured (open circles) neutron multiplicity as a function of the total excitation energy of the fragments averaged over 8 u around the projectile (upper part) and the target (lower part) masses. The hatched areas are calculations based on the code JULIAN (Ref. 40), the dashed line is the result of a calculation based on the code EVA (Ref. 47). All calculations were performed for ^{86}Kr (upper part) and ^{166}Er (lower part).

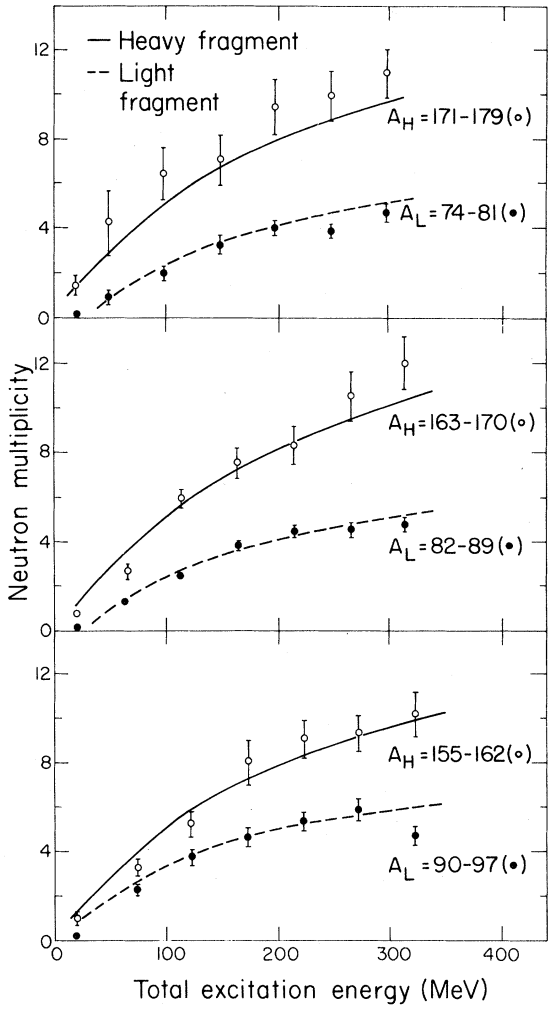

FIG. 14. Measured neutron multiplicities as a function of total excitation energy of the fragments for various mass bins. The solid (dashed) line represents calculations of neutron multiplicity based on the code EVA[47] for the H (L) fragment. The calculations were done for the mean value of the mass bin.

takes angular momentum explicitly into account. Angular momentum dependent decay widths for n, p, and α particles were computed according to the Hauser-Feshbach formalism. In addition, γ ray and fission were included. Transmission coefficients were calculated from optical potentials taken from Refs. 41 and 42. γ-ray transitions up to multipolarity 2 were taken into account using empirical transition strengths from Ref. 43. The fission width was calculated as described in Ref. 44, using rotating-liquid-drop fission barriers.[45] Level densities were calculated with the formalism of Gilbert and Cameron,[46] with the level density parameter $a = A/8$.

The results are shown in Fig. 13 (hatched area) for ^{86}Kr and ^{166}Er as a function of the total excitation energy for extreme values of the angular momentum of the fragments. It is seen that the neutron multiplicity varies only weakly with the fragment spin. The variations are comparable to or smaller than the experimental uncertainty of the neutron multiplicity. The dashed line in Fig. 13 shows the results of calculations using the much simpler code EVA.[47] Good agreement is evident between the two codes. Since the calculations become prohibitively along with the code JULIAN, especially for high masses at high excitation energies, all other calculations were performed using the much faster code EVA.

The comparison of these calculations with the experimental multiplicities shows a significant disagreement at high excitation energies (Fig. 13), the calculated multiplicities being higher than the measured ones. Much better agreement is obtained using the value $a = A/20$ for the level density parameter,[47] as can be seen in Fig. 14. It was

shown in Ref. 47 that this value of the level density parameter gave a very good fit to evaporation cross sections for a large number of reactions covering a wide range of excitation energies and target nuclei. With this value of "a," the code predicts a higher charged particle multiplicity at high excitation energies (and therefore a lower neutron multiplicity), and it reproduces quite well the change in slope of the experimental multiplicities. The agreement between the measured and the calculated multiplicities confirms that the excitation energy is shared between the fragments in proportion to their mass, i.e., the composite system reaches thermal equilibrium prior to the separation of the fragments. Similar conclusions were also obtained in our previous study at lower bombarding energies.[1,2]

V. A POSSIBLE MECHANISM FOR PREEQUILIBRIUM NEUTRON EMISSION

In the last section we showed that the neutron angular distribution and velocity spectra cannot be reproduced with the assumption that all neutrons are isotropically evaporated from the fully accelerated fragments. There are discrepancies which we interpret as evidence for preequilibrium neutron emission. These preequilibrium neutrons have the following characteristics: They are emitted close to the L-fragment direction in quasielastic events and close to the H-fragment direction in deep inelastic events. If one associates quasielastic events with positive deflection angles and deep inelastic events with negative deflection angles,[48] it is possible to understand these observations assuming the preequilibrium neutrons are emitted at an early stage of the collision as illustrated in Fig. 15; in the approaching phase, preequilibrium neutrons are knocked out at the contact point, in the direction of the nuclear trajectory. These neutrons are emitted at positive angles close to the L fragment for quasielastic events and at negative angles, due to the nuclear orbiting, for deep inelastic events. This picture has also been proposed in Ref. 49.

In order to further test this interpretation we wrote a Monte Carlo simulation code in which we made the following specific assumptions about the preequilibrium neutron emission:

(i) The preequilibrium neutrons are emitted in the approach phase of the collision, at the "contact" point defined by R_p+R_T+2a, where R_P and R_T are the projectile and target radii, respectively, and a is the nuclear diffuseness taken as 0.6 fm.

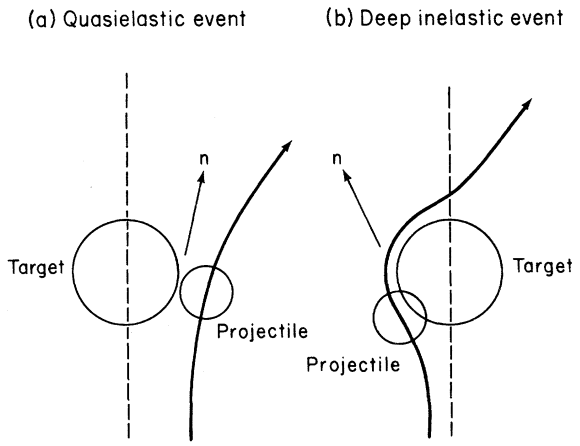

FIG. 15. Schematic illustration of the mechanism of preequilibrium neutron emission in quasielastic (a) and deep inelastic (b) events.

(ii) The preequilibrium neutrons are emitted along the direction of the tangential nuclear motion. Their velocity is taken to be equal to the relative nuclear velocity at the point of contact. These are taken as the mean values $\bar{\theta}$ and $\bar{v}$ of Gaussian distributions with standard deviations $\sigma_{\bar{\theta}}=15°$ and $\sigma_{\bar{v}}=1.7$ cm/ns, respectively. The values of $\bar{\theta}$ and $\bar{v}$ were obtained as a function of TKE from the trajectories calculated using the classical friction model of Gross and Kalinowski.[50]

(iii) The preequilibrium neutrons represent a constant fraction f (independent of the mass and TKE of the fragments) of the total number of neutrons. The calculations presented here were performed with the value $f=0.1$.

The Wilczinski plot predicted by the model of Gross and Kalinowski[50] is indicated in Fig. 5 by the dashed line. It reproduces qualitatively the experimental ridge but the calculated energy loss is too small. The inclusion of nuclear deformation in the exit channel improves the agreement,[50] however it has little effect on the parameters $\bar{\theta}$ and $\bar{v}$.[51]

The inputs of the code are the measured angular, mass, and TKE distributions of the fragments, the measured L- and H-fragment neutron multiplicities, and the averaged neutron c.m. energy spectra of Fig. 12. The code then proceeds in the following sequence: It chooses randomly an event out of the input distributions. Ninety percent of all neutrons are isotropically emitted in the rest frame of the fragments, the remaining 10% are emitted according to the prescription of preequilibrium emission described above. The code uses exactly the same geometry as in the real experiment in order to detect

neutron-fragment coincidences. These simulated data are finally analyzed as described in Sec. III, i.e., assuming *all* neutrons were statistically evaporated from the fully accelerated fragments.

The angular distribution and the velocity spectra of the neutrons obtained from the simulation calculations are presented in Figs. 16 and 17, respectively. These figures are to be compared to Figs. 7—11 which show the same information for the real experiment. This comparison shows that the inclusion of the preequilibrium neutrons in the simulation reproduces qualitatively the effects observed in the experiment. We did not try to adjust the parameters of the preequilibrium neutrons in order to obtain a better fit. The essential point here is that this simple mechanism of preequilibrium emission reproduces the observed effects. It is interesting to note that although the preequilibrium neutrons are included in the simulation for all TKE values, they do manifest themselves in the analysis only for quasielastic and strongly damped events.

We varied the parameters f and σ_θ, which play an important role in the neutron angular distribution, in order to get a feeling of the sensitivity of the calculations in determining the fraction f of preequilibrium neutrons. These variations showed that the total amount of preequilibrium neutrons is relatively small, in the range of 5—15 %.

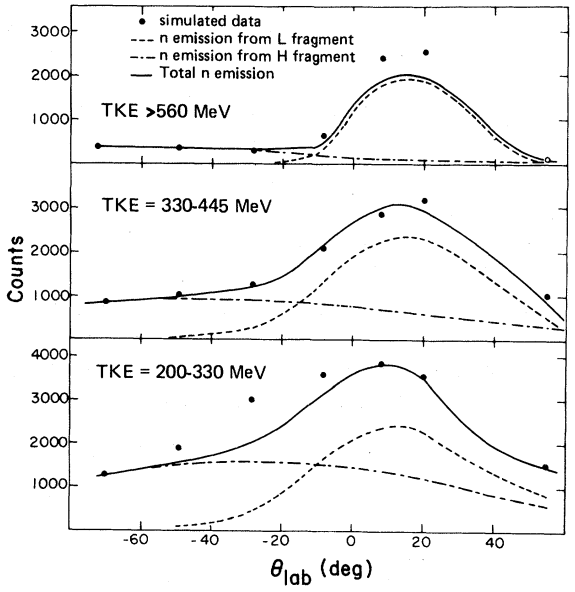

FIG. 16. Neutron angular distribution in the laboratory system obtained with a Monte Carlo simulation code which includes preequilibrium neutron emission (see text). The lines were obtained by applying to the simulated data (dots) the same analysis as in the real experiment, i.e., assuming that *all* neutrons were isotropically emitted in the rest frame of the fragments. Compare to Fig. 7.

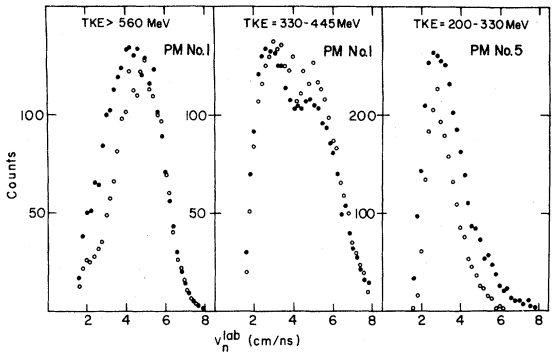

FIG. 17. Simulated (closed circles) neutron velocity spectra from the simulation code which includes preequilibrium neutron emission (see text). The open points were calculated from the simulated spectra in the reference counters, assuming that *all* neutrons were isotropically emitted in the c.m. system of the fragments. Compare to Figs. 8, 9, and 11.

VI. SUMMARY

We have reported a study of neutron emission associated with deep inelastic collisions of ^{86}Kr on ^{166}Er at 1.02 GeV. Neutrons were detected in coincidence with the two complementary heavy reaction fragments. The measurement of the velocities and scattering angles of the fragments allowed the determination of the primary masses and kinetic energies of the fragments. The neutron velocity spectra were determined as a function of TKE and neutron scattering angles. Neutron c.m. energy spectra and neutron multiplicities were obtained from two reference counters as functions of TKE and mass of the fragments.

Our data analysis shows that the neutron angular distribution and velocity spectra cannot be accounted for by assuming only isotropic emission from the fully accelerated fragments. There is evidence for preequilibrium neutrons which are emitted on the side of the L fragment with respect to the beam axis in quasielastic events and on the side of the H fragment in strongly damped events. Contrary to the predictions of some theoretical models, the preequilibrium neutrons do not have high velocities; they have a broad velocity distribution centered at a velocity smaller or close to the beam velocity.

We have proposed a simple picture for preequilibrium neutron emission in which a fraction of the

neutrons are knocked out at an early stage of the collision, along the direction of the projectile motion. Simulation calculations show that this picture qualitatively reproduces the effects observed in the experiments and that the preequilibrium neutrons represent 5–15 % of all neutrons emitted

The small fraction of preequilibrium neutrons does not affect the c.m. energy spectra and the neutron multiplicities. The neutron c.m. energy spectra indicate that the excitation energy is shared between the fragments in proportion to their mass and that the composite system is equilibrated prior to the separation of the fragments. The observed neutron multiplicities as a function of mass and TKE of the fragments are in good agreement with predictions of statistical model calculations.

APPENDIX

In this appendix we describe in detail the procedure used in the event-by-event analysis of the neutron-fragment coincidence data. As explained in Sec. III B, the analysis is based on the assumption that all neutrons originate from the L or the H fragment and that they are isotropically evaporated in the rest frame of the fragments. The c.m. spectra of the neutrons emitted from these two sources are calculated from the measured neutron spectra in two reference counters located close to the directions of the L and H fragments. This calculation is based only on the "high" velocity neutrons, i.e., those which are emitted in the forward direction in the rest frame of the fragment. Thus when a neutron is detected in the reference counter PM No. 2 (or PM No. 7) it is first assumed that the neutron originated from the L (or H) fragment and it is accepted in the analysis if the following condition is fulfilled:

$$v_n \geq v_F \cos\theta_n \ , \tag{1}$$

where v_n is the neutron velocity in the reference counter, v_F is the velocity of the fragment detected close to the reference counter, and θ_n is the angle between the neutron and the fragment directions (see the velocity diagram of Fig. 18). Figure 19 shows the measured neutron velocity spectra in the reference counter PM No. 2 (solid circles). The dashed lines indicate the "accepted" neutrons, i.e, those fulfilling Eq. (1). It is seen that more than 60% of the detected neutrons are used in the analysis.

The neutron velocity in the rest frame of the fragment is obtained from

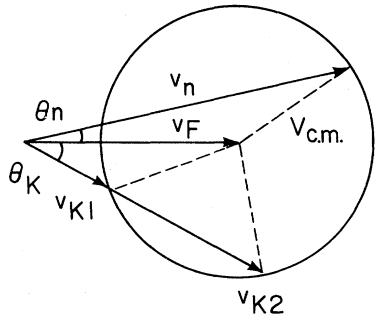

FIG. 18. Velocity diagram of neutron emission.

$$v_{\text{c.m.}} = (v_n^2 + v_F^2 - 2v_n v_F \cos\theta_n)^{1/2} \ . \tag{2}$$

The event is then stored in the array of c.m. events $N_{\text{c.m.}}(v_{\text{c.m.}}, M, \text{TKE}, J)$, where J denotes the reference counter (PM No. 2 or 7) and M is the mass of the L fragment. The event is assigned a weight given by

$$W_{\text{c.m.}} = \frac{v_{\text{c.m.}}(v_n - v_F \cos\theta_n)}{v_n^2} \frac{4\pi}{\epsilon_n \Delta\Omega_n} \ , \tag{3}$$

where ϵ_n and $\Delta\Omega_n$ are the detection efficiency and the solid angle of the reference counter, respectively. This weight is determined by the Jacobian of the transformation from the laboratory system to the c.m. system and the assumption of isotropic emission.

The next step is to project this event back into the laboratory system and to evaluate its contribution in each of the eight neutron counters. This event contributes to PM No. K if

$$v_{\text{c.m.}} \geq v_F \sin\theta_K \ , \tag{4}$$

where θ_K is the angle between the fragment and PM No. K. If this condition is fulfilled there are one or two solutions for the projected neutron velocity in PM No. K corresponding to this event:

$$v_K = v_F \cos\theta_K \pm (v_{\text{c.m.}}^2 - v_F^2 \sin^2\theta_K)^{1/2} \ . \tag{5}$$

Both solutions are stored in the array of projected events $N_p(v_K, K, J)$ with a weight

$$W_K = \frac{v_n - v_F \cos\theta_n}{v_K - v_F \cos\theta_K} \frac{v_K^2}{v_n^2} \frac{\epsilon_K \Delta\Omega_K}{\epsilon_n \Delta\Omega_n} \ . \tag{6}$$

If K is the opposite reference counter the whole procedure is repeated from Eq. (1) with the following values: v_K is the neutron velocity in the reference counter, v_F' is the velocity of the complementary fragment, and θ_K is the angle between these two

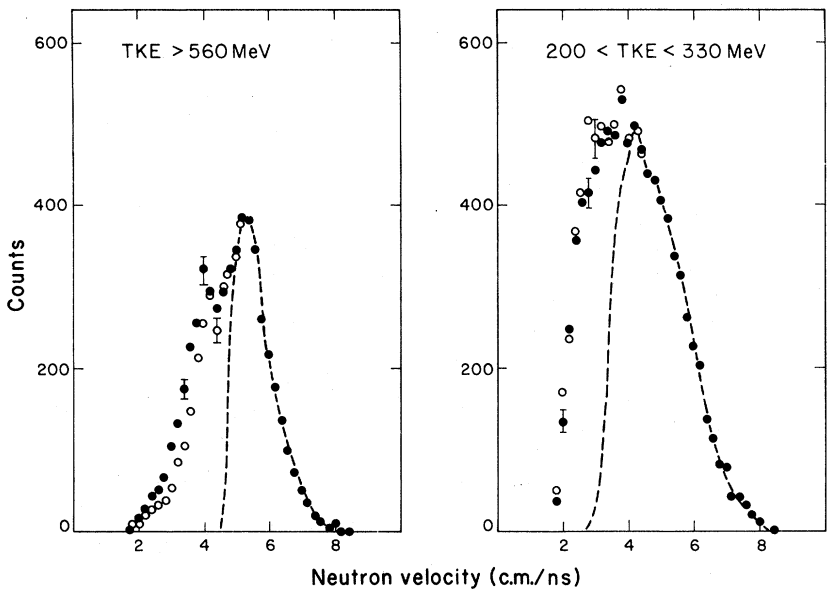

FIG. 19. Neutron velocity spectra measured (closed circles) in the reference counter PM No. 2. The dashed lines show the yield of neutrons which satisfy Eq. (1). The open circles represent the calculated yield assuming isotropic emission in the c.m. system of the fragments.

directions. The event is assigned an initial weight $-W_K$. This iteration procedure converges rapidly, generally after one iteration, due to the condition expressed by Eq. (1), and it corrects for the neutrons detected in PM No. 2 which were emitted by the H fragment. The projected spectra on the reference counters identically reproduces the high velocity branch of the measured spectra [this is obvious from the construction procedure, $W_K=1$ in Eq. (6), when K is the reference counter and v_K is the high velocity solution of Eq. (5)]. The comparison of the measured and projected spectra of the reference counters is meaningful only for the low velocity part of the spectra. This comparison provides information about the forward-backward symmetry of the neutron emission in the rest frame of the fully accelerated fragment. The projected low-velocity neutrons in PM No. 2 are shown in Fig. 19 by the open circles. It is seen that for quasielastic events, TKE $>$ 560 MeV, the measured spectrum is larger than the projected one. This explains why the total calculated neutron yield in Fig. 7 does not reproduce the yield measured in the primary counter PM No. 2. The effect is very similar to the one observed in PM No. 1 in Fig. 9 and demonstrates that the preequilibrium neutrons are also present in the reference counter. For strongly damped events, TKE $=200-330$ MeV, there is good agreement between the measured and the calculated low-velocity spectra of the neutrons in PM No. 2 as shown in Fig. 19. In this case the spectrum is consistent with forward-backward symmetry of neutron emission.

*Deceased.

[1]Y. Eyal, A. Gavron, I. Tserruya, Z. Fraenkel, Y. Eisen, S. Wald, R. Bass, C. R. Gould, G. Kreyling, R. Renfordt, K. Stelzer, R. Zitzmann, A. Gobbi, U. Lynen, H. Stelzer, I. Rode, and R. Bock, Phys. Rev. Lett. 41, 625 (1978).

[2]Y. Eyal *et al.*, Phys. Rev. C 21, 1377 (1980).

[3]D. Hilscher, J. R. Birkelund, A. D. Hoover, W. U. Schroder, W. W. Wilcke, J. R. Huizenga, A. Mignerey, K. L. Wolf, H. F. Breuer, and V. E. Viola, Jr., Phys. Rev. C 20, 576 (1979).

[4]B. Tamain, R. Chechik, H. Fuchs, F. Hanappe, M. Morjean, C. Ngo, J. Peter, M. Dakowski, B. Lucas, C. Mazur, M. Ribrag, and C. Signarbieux, Nucl. Phys. A330, 253 (1979).

[5]C. R. Gould, R. Bass, J. V. Czarnecki, V. Hartmann, K. Stelzer, R. Zitzmann, and Y. Eyal, Z. Phys. A 294, 323 (1980).

[6]A. Gamp, J. C. Jacmart, N. Poffe, H. Doubre, J. C. Roynette, and J. Wilczinski, Phys. Lett. 74B, 215 (1978).

[7]J. M. Miller, G. L. Catchen, D. Logan, M. Rajagopalan,

J. M. Alexander, M. Kaplan, and M. Zisman, Phys. Rev. Lett. 40, 100 (1978).
[8]D. Logan, H. Delagrange, M. F. Rivet, M. Rajagopalan, J. M. ALexander, M. Kaplan, M. S. Zisman, and E. Duek, Phys. Rev. C 22, 1080 (1980).
[9]In a recent work L. G. Sobotka *et al.* have shown that in the system ^{165}Ho + ^{181}Ta at 8.2 MeV/nucleon the dominant sources of α particles are the fully accelerated fragments. Lawrence Berkeley Laboratory Report LBL-13319, 1982 (unpublished).
[10]H. Ho, R. Albrecht, W. Dunnweber, G. Graw, S. G. Steadman, J. P. Wurm, D. Disdier, V. Rauch, and F. Scheibling, Z. Phys. A 283, 235 (1977).
[11]J. W. Harris, J. M. Cormier, D. F. Geesaman, L. L. Lee, Jr., R. L. McGrath, and J. P. Wurm, Phys. Rev. Lett. 38, 1460 (1977).
[12]R. K. Bhowmik, E. C. Pollacco, N. E. Sanderson, J. B. A. England, and G. C. Morrison, Phys. Rev. Lett. 43, 619 (1979).
[13]R. Billerey, C. Cerruti, A. Chevarier, N. Chevarier, B. Cheynis, and D. Demeyer, Z. Phys. A 292, 293 (1979).
[14]H. Gemmeke, P. Netter, A. Richter, L. Lassen, S. Lewandowski, W. Lucking, and R. Schreck, Phys. Lett. 97B, 213 (1980).
[15]A. Gavron, R. L. Ferguson, F. E. Obenshain, F. Plasil, G. R. Young, G. A. Petitt, K. A. Geoffroy, D. G. Sarantites, and C. F. Maguire, Phys. Rev. Lett. 46, 8 (1981).
[16]R. L. Robinson, R. L. Auble, I. Y. Lee, M. J. Martin, G. R. Young, J. Gomez del Campo, J. B. Ball, F. E. Bertrand, R. L. Ferguson, C. B. Fulmer, J. R. Wu, J. C. Wells, and H. Yamada, Phys. Rev. C 24, 2084 (1981).
[17]S. Wald, I. Tserruya, Z. Fraenkel, G. Doukellis, H. Gemmeke, and H. L. Harney, Phys. Rev. C 25, 1118 (1982).
[18]M. B. Tsang, W. G. Lynch, R. J. Puigh, R. Vandenbosch, and A. G. Seamster, Phys. Rev. C 23, 1560 (1981).
[19]M. Bini, C. K. Gelbke, D. K. Scott, T. J. M. Symons, P. Doll, D. L. Hendrie, J. L. Laville, J. Mahoney, M. C. Mermaz, C. Olmer, K. Van Bibber, and H. H. Wieman, Phys. Rev. C 22, 1945 (1980).
[20]G. R. Young, R. L. Ferguson, A. Gavron, D. C. Hensley, F. E. Obenshain, F. Plasil, A. H. Snell, M. P. Webb, C. F. Maguire, and G. A. Petitt, Phys. Rev. Lett. 45, 1389 (1980).
[21]H. Ho, R. Albrecht, H. Damjantschitsch, F. J. Demond, W. Kuhn, J. Slemmer, J. P. Wurm, D. Disdier, V. Raugh, F. Scheibling, and T. Dossing, Z. Phys. A 300, 205 (1981).
[22]R. Babinet, B. Cauvin, J. Girard, J. M. Alexander, T. H. Chiang, J. Galin, B. Gatty, D. Guerreau, and X. Tarrago, Z. Phys. A 295, 153 (1980).
[23]W. Kuhn, R. Albrecht, H. Damjantschitsch, H. Ho, R. M. Ronningen, J. Slemmer, J. P. Wurm, I. Rode, and F. Scheibling, Z. Phys. A 298, 95 (1980).
[24]P. A. Gottschalk and M. Westrom, Phys. Rev. Lett. 39, 1250 (1977).
[25]R. Weiner and M. Westrom, Nucl. Phys. A286, 282 (1977).
[26]P. A. Gottschalk and M. Westrom, Nucl. Phys. A314, 232 (1979).
[27]S. I. A. Garpman, D. Sperber, and M. Zielinska-Pfabe, Phys. Lett, 90B, 53 (1980).
[28]J. P. Bondorf, J. N. De, A. O. T. Karvinen, G. Fai, and B. Jakobson, Phys. Lett. 84B, 162 (1979).
[29]J. P. Bondorf, J. N. De, G. Fai, A. O. T. Karvinen, B. Jakobson, and J. Randrup, Nucl. Phys. A333, 285 (1980).
[30]W. J. Swiatecki, Lawrence Berkeley Laboratory Report LBL-8950, 1979 (unpublished).
[31]D. H. E. Gross, Nucl. Phys. A240, 472 (1975).
[32]D. H. E. Gross and J. Wilczinski, Phys. Lett. 67B, 1 (1977).
[33]I. Tserruya, A. Breskin, R. Chechik, Z. Fraenkel, S. Wald, N. Zwang, R. Bock, M. Dakowski, A. Gobbi, H. Sann, R. Bass, G. Kreyling, R. Renfordt, K. Stelzer, and U. Arlt, Phys. Rev. Lett. 47, 16 (1981).
[34]Y. Eyal and H. Stelzer, Nucl. Instrum. Methods 155, 157 (1978).
[35]A. Olmi, U. Lynen, J. B. Natowitz, M. Dakowski, P. Doll, A. Gobbi, H. Sann, H. Stelzer, R. Bock, and D. Pelte, Phys. Rev. Lett. 44, 383 (1981).
[36]M. Drosg, Nucl. Instrum. Methods 105, 582 (1972).
[37]U. Lynen (unpublished).
[38]Z. Fraenkel, I. Mayk, J. P. Unik, A. J. Gorski, and W. D. Loveland, Phys. Rev. C 12, 1809 (1975).
[39]Y. Eyal, G. Rudolf, I. Rode, and H. Stelzer, Phys. Rev. Lett. 42, 826 (1979).
[40]JULIAN, Monte Carlo statistical-model code, H. Hillman and Y. Eyal (unpublished), modified by A. Gavron to couple angular momentum projections.
[41]L. Rosen, J. G. Beerg, A. S. Goldhaber, and E. H. Auerbach, Ann. Phys. (N.Y.) 34, 96 (1965); C. M. Perey and F. G. Perey, Nucl. Data Tables 17, 1 (1976).
[42]J. R. Huizenga and G. Igo, Nucl. Phys. 29, 462 (1962).
[43]F. Bertrand, M. Martinot, and N. Verges, in *Nuclear Data in Science and Technology* (IAEA, Vienna, 1973), Vol. II, p. 353.
[44]A. M. Zebelman, L. Kowalski, J. Miller, K. Beg, Y. Eyal, G. Yaffe, A. Kandil, and D. Logan, Phys. Rev. C 10, 200 (1974).
[45]S. Cohen, F. Plasil, and W. J. Swiatecki, Ann. Phys. (N.Y.) 22, 406 (1973).
[46]A. Gilbert and A. G. W. Cameron, Can. J. Phys. 43, 1446 (1965).
[47]I. Dostrovsky, Z. Fraenkel, and G. Friedlander, Phys. Rev. 116, 683 (1959).
[48]J. Wilczinski, Phys. Lett. 47B, 484 (1973).
[49]C. K. Gelbke, M. Bini, C. Olmer, D. L. Hendrie, J. L. Laville, J. Mahoney, M. C. Mermaz, D. K. Scott, and H. H. Wieman, Phys. Lett. 71B, 83 (1977).
[50]D. H. E. Gross and H. Kalinowski, Phys. Rep. 45, 175 (1978).
[51]D. H. E. Gross, private communication.